Highly Luminescent Zinc(II)−Bis(8-hydroxyquinoline) Complex Nanorods: Sonochemical Synthesis, Characterizations, and Protein Sensing

Hong-Cheng Pan,[†] Fu-Pei Liang,[†,‡] Chang-Jie Mao,[†] Jun-Jie Zhu,*[,†] and Hong-Yuan Chen[†]

Key Lab of Analytical Chemistry for Life Science (MOE), School of Chemistry and Chemical Engineering, Nanjing University, Nanjing 210093, China, and School of Chemistry and Chemical Engineering, Guangxi Normal University, Guilin 541004, China

Received: January 14, 2007; In Final Form: March 11, 2007

Highly luminescent zinc(II)−bis(8-hydroxyquinoline) (Znq_2) complex nanorods have been synthesized via a sonochemical route from the microemulsion containing zinc acetate and 8-hydroxyquinoline. The scanning electron microscopy (SEM) and transmission electron microscopy (TEM) images showed that the products were rod-like morphology with a diameter of about 200−450 nm and a length of about 1−3 μm. A possible mechanism for the formation of Znq_2 nanorods is proposed that the ultrasound wave might urge the collision and fusion of initial Znq_2 nuclei to form nanorods. The photoluminescence (PL) and resonance light scattering (RLS) of the products were also investigated. The Znq_2 nanorods were found to be sensitive to several proteins, such as human serum albumin (HSA), bovine serum albumin (BSA), bovine hemoglobin (Hb), and egg albumin (EA), displaying an increase in intensities of both PL and RLS. The protein-concentration dependence of the PL and RLS intensities can be well described as a Langmuir-type binding isotherm. This is the first report on the enhancement of PL and RLS intensities of Znq_2 nanorods by proteins. On the basis of enhanced PL and RLS intensities, the protein could be detected at the nanogram per milliliter level. The experimental results clearly showed that the Znq_2 nanorods were good protein probes for easy and highly sensitive detection.

Introduction

Recently several types of luminescent nanoparticles, such as quantum dots,[1−3] fluorophore doped silica nanoparticles,[4] Europium-chelate incorporated polystyrene nanoparticles,[5] and upconversion fluorescence nanocrystals,[6−8] have been explored as fluorescent probes for fluorescence imaging and bioanalysis. Increasing attention is currently being devoted to the development of complex-based nanoparticles for luminescence applications, due to their high quantum yield and multifunctional groups that provide affinity sites for the binding of biomolecules.[9−14] As a type of highly luminescent and electroluminescent material, zinc(II)−bis(8-hydroxyquinoline) (Znq_2) is becoming the subject of intense interest because of its use in low-voltage organic light-emitting devices (OLEDs). However, its potential applications in bioanalytical science are still at an early stage, in comparison with their extensive applications in OLEDs. The rapid advances in nanotechnology are creating new opportunities for the applications of Znq_2 in the field of bioanalysis and biosensors. Recently, the studies on Znq_2 have shown that the metal chelate forms a supramolecular tetrameric structure composed of a Zn_4O_8 core via oxo-bridging of the 8-quinolinolato ligands.[15,16] Thus, it is reasonable to expect that the preferential directional growth of Znq_2 supramolecular structure may form a one-dimensional (1D) nanostructure. Generally, nanostructured films of metal−quinoline chelates (e.g., Alq_3) can be synthesized by vacuum-deposited methods.[17−20] However, there are no reports on the preparation Znq_2 by this method. An alternative method for the preparation of nanoparticles is the wet chemistry approach, which is simple and inexpensive compared to physical vapor deposition. In the previous work, we have concentrated on the applications of the sonochemical approach to the synthesis of inorganic nanoparticles with different morphologies, such as heterostructured Bi_2Se_3 nanowires, CdSe hollow spherical assemblies, $BiPO_4$ nanorods, $PbWO_4$ nanocrystals, Bi_2S_3 nanorods, gold nanorings, $Cd(OH)_2$ nanorings, and self-assembled V_2O_5 bundles.[21−28] However, to our knowledge, there are no reports for the preparation of Znq_2 nanorods by the sonochemical method.

In the present work, we combined the sonochemical method with the microemulsion technique to prepare the highly luminescent 1D Znq_2 complex nanorods. This was found to be a feasible, rapid, mild, and energy efficient method for the preparation of the Znq_2 nanorods with a diameter of 200−450 nm and a length of 1−3 μm. We have focused on understanding the formation mechanism of Znq_2 nanorods. The results showed that the ultrasound wave might urge the collision and fusion of initial Znq_2 nuclei to form nanorods. We have also investigated the optical properties of the composites, as well as the binding of proteins to the nanorods by means of photoluminescence (PL) and resonance light scattering (RLS). Interestingly, the Znq_2 nanorods were found to be sensitive to several proteins such as human serum albumin (HSA), bovine serum albumin (BSA), bovine hemoglobin (Hb), and egg albumin (EA), displaying the increase in intensities of both PL and RLS. The protein-concentration dependence of the PL and RLS intensities can be well described as a Langmuir-type binding isotherm. As far as we know, this is the first such report to show that some proteins can enhance the PL and RLS of Znq_2 nanorods. The findings have encouraged us to develop an optical strategy based on the Znq_2 nanorods for protein sensing.

* Address correspondence to this author. Fax: +86-25-83594976. E-mail: jjzhu@nju.edu.cn.
[†] Nanjing University.
[‡] Guangxi Normal University.

10.1021/jp0703049 CCC: $37.00
Published on Web 04/27/2007

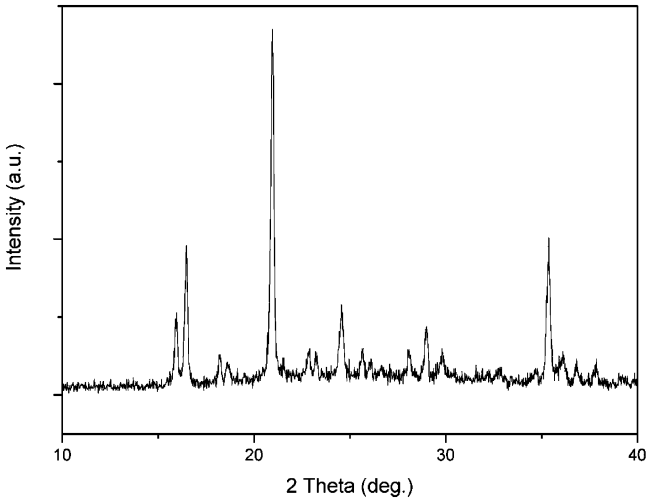

Figure 1. XRD pattern of the Znq_2 nanorods.

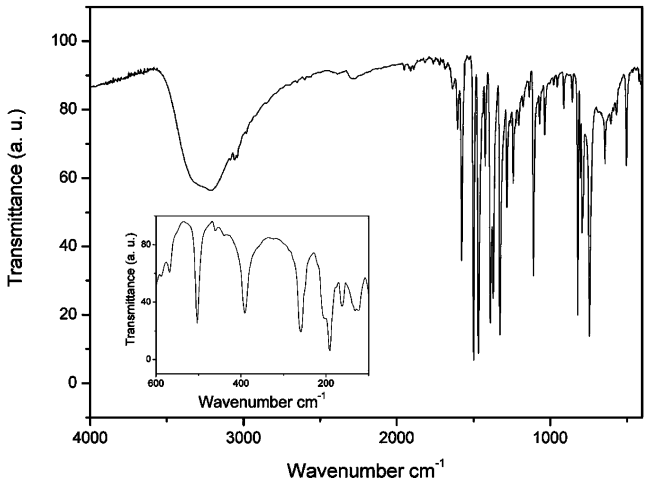

Figure 2. IR spectrum of the Znq_2 nanorods. Inset: Far-IR spectrum.

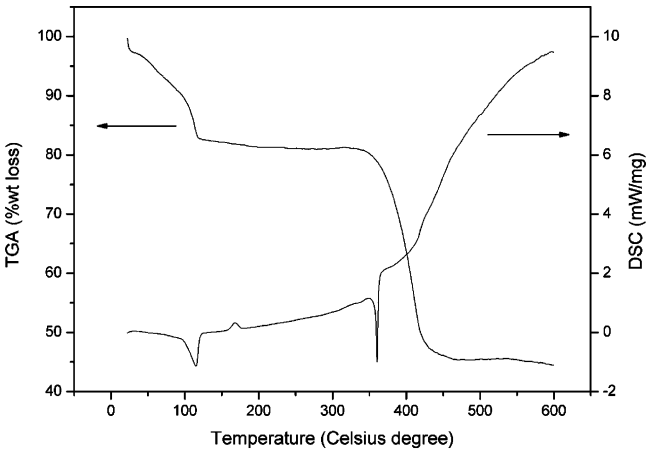

Figure 3. Thermal analysis of the Znq_2 nanorods.

Experimental Section

Materials. 8-Hydroxyquinoline was purchased from Beijing Solarbio (China). Zinc acetate and bovine hemoglobin (Hb) were purchase from Beijing Chemical Reagents Company (China). Human serum albumin (HSA) was obtained from Sigma. Egg albumin (EA) was purchased from Shanghai Bio life (China). Bovine serum albumin (BSA) was obtained from Nanjing Genetime Bio (China). Doubly distilled water was used throughout.

Preparation of Zinc(II)−Bis(8-hydroxyquinoline) Nanorods. The nanorods were prepared by using a sonochemical method combined with a microemulsion technique. A water-in-oil (W/O) microemulsion was prepared by mixing TX-100 (30 mL), cyclohexane (55 mL), *n*-hexanol (15 mL), 0.2 M zinc acetate aqueous solution (2.5 mL), and ethanol (2.5 mL). 8-Hydroxyquinoline (1.5 mmol, 0.2175 g) was dissolved in ethanol/water solution (50%, v/v, 5 mL) and then was added into the microemulsion. The mixture solution was exposed to the high-intensity ultrasound irradiation under ambient air for 45 min. Ultrasound irradiation was accomplished with a high-intensity ultrasonic probe (Xinzhi Co., Xinzhi, China; 1.2 cm diameter; Ti-horn, 20 kHz, 100 W cm^{-2}) immersed directly in the reaction solution. When the reaction was finished, a yellowish-green precipitate was obtained. After cooling to room temperature, the precipitate was separated by centrifuging at a rotation rate of 9000 rounds per min. It was purified further by repeated cycles of centrifuge and dispersing in ethanol and then dried in air at room temperature. The final products were redispersed in 50% (v/v) glycerol/water solution for further usage.

Characterization. The products were characterized by X-ray diffraction (XRD; Philip X'pert X-ray diffractometer with Cu Kα radiation, $\lambda = 1.5418$ Å), field-emission scanning electron microscope (FE-SEM; LEO-1530VP), and transmission electron microscope (TEM; JEOL-JEM 200CX). The infrared (IR) spectra were obtained with a Nicolet Nexus 870 FT-IR spectrophotometer. Elemental analysis (EA) was carried out with a Heraeus CHN-O Rapid instrument. Thermal gravimetric analysis (TGA) and differential scanning calorimetry (DSC) were performed with a Netzsch 409 Simultaneous Thermal Analyzer (STA) system. The samples were placed in an Al_2O_3 crucible and heated at a rate of 5 deg/min under N_2 gas at a flow rate of 25 mL min^{-1}. Photoluminescence (PL) spectra were recorded on a Shimadzu RF-5301PC spectrofluorophotometer. Light-scattering studies were performed on a Shimadzu RF-5301PC spectrofluorophotometer at a 90° scattering angle. The resonance light scattering (RLS) spectra were obtained by synchronously scanning the excitation and emission monochromators in the wavelength region from 300 to 900 nm (namely, $\lambda_{ex} = \lambda_{em}$). All spectra were collected at room temperature.

Results and Discussion

Characterizations of the Products. The X-ray diffraction (XRD) of the as-prepared product is shown in Figure 1. The diffraction peaks can be indexed to be zinc(II)−bis(8-hydroxyquinoline) (JCPDS card no. 48−2116). The water of hydration in the samples was readily identified by the presence of a broad infrared absorption band in the region from 3000 to 3400 cm^{-1}, as shown in Figure 2. The intensity ratio of 3333 cm^{-1} band to 1110 cm^{-1} band is commonly used to study the water molecule number in metal−quinoline chelates. The intensity ratio (0.593) in the present work indicated that the product was Znq_2 dihydrate, which is in good agreement with previous reports.[29] The vibrations at 1605, 1577, 1391, and 1328 cm^{-1} were assigned to the quinoline group of Znq_2. The bands at 1500 and 1468 cm^{-1} should correspond to both the pyridyl and phenyl groups in Znq_2.[30] The peaks at 744, 642, and 605 cm^{-1} were associated with in-plane ring deformation.[31] In the far-IR region as shown in the inset of Figure 2, the peaks at 391 and 202 cm^{-1} were associated with the Zn−O stretching vibration and the Zn−N stretching vibration.[32] The EA results of the sample showed that the content (%) of C, N, and H was 54.66, 7.04, and 4.01, respectively. The values are consistent with the

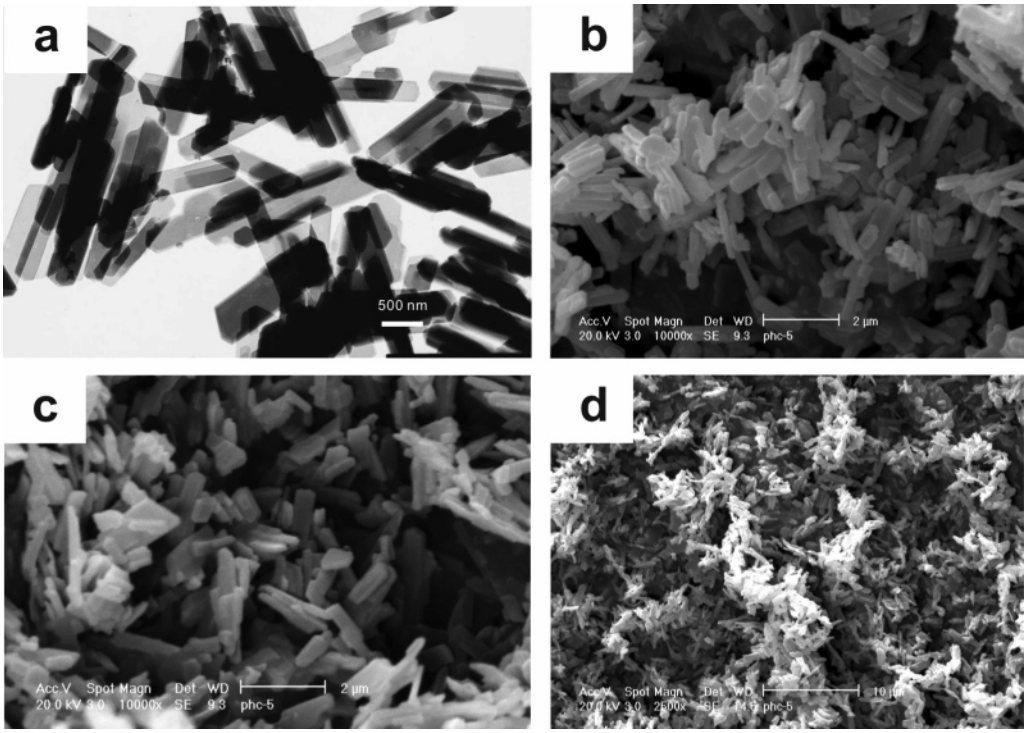

Figure 4. TEM and SEM images of the Znq_2 nanorods.

calculated values (C 55.47%; N 7.19%; H 4.14%) and the product can be confirmed to be Znq_2 dihydrate.

Figure 3 shows the TGA and DSC results for the Znq_2 nanorods. The first weight loss step occurs up to 120 °C in the TGA curve and it is ascribed to the loss of water. An endothermic peak at 117 °C in the DSC curve also corresponded to the water loss process of Znq_2 dihydrate. After water loss, an endothermic peak at 360 °C and decomposition of the sample at ∼440 °C were observed, which are consistent with the literature.[15] According to the experimental data the composition of the product can be confirmed to be the Znq_2 dihydrate.

The size and morphology of the Znq_2 nanorods were examined by TEM and FE-SEM. A typical TEM image shown in Figure 4a reveals that the products are rod-like morphology with diameters of 200−450 nm and lengths of about 1−3 μm. The SEM image in Figure 4b,c,d further confirms that the products are nanorods.

Effect of Ultrasound Irradiation and Possible Formation Mechanism. In the case of a microemulsion, 8-hydroxyquinoline reacted with Zn^{2+} in the core of the microemulsions and the hydrophilic head groups of the surfactant molecules. A liquid−solid heterogeneous system was formed after nucleation of the Znq_2 nuclei. When ultrasound was applied to the system, the generated bubbles collapse asymmetrically. This mode of asymmetric collapse resulted in the formation of high-speed microjets of liquids as well as shockwaves that drive the solid particles to high velocities, which led to interparticle collisions. The effects of interparticle collisions, microjets, and shockwaves could push the Znq_2 nanoparticles toward each other, forming the nanorods. Here, ultrasound irradiation played a crucial role and was found to be necessary to the synthesis of Znq_2 nanorods. Comparative experiments were performed under vigorous electromagnetic stirring instead of ultrasonic treatment where only nanosized particles can be obtained. Therefore, in the reaction, the ultrasound wave might urge the collision and fusion of initial Znq_2 nuclei to form nanorods.

Time-dependent experiments were performed to gain an insight into the formation process of the sample. The products were characterized by TEM at different irradiation times, which correspond to the particular status of the microemulsion. TEM images obtained after different reaction times showed an obvious growth process from small primary nanoparticles to the final rod-like shape. Figure 5 shows the images taken from the reaction mixture after the solution was exposed to high-intensity ultrasound irradiation for 1, 3, 6, 12, and 40 min. In Figure 5a, TEM images of the early growth stage of Znq_2 showed that the spherical Znq_2 nanoparticles were obtained after ultrasound irradiation for 1 min. With the ultrasound proceeding, the formed Znq_2 nanoparticles underwent fusion to form the small rods composed of small particles (Figure 5b,c), confirming the particles have been integrated by droplets collision and fusion. Further ultrasound irradiation (over 10 min) led to the continuous growth of Znq_2 nanorods (Figure 5d,e). To make a comparison, we have also carried out the reaction with vigorous electromagnetic stirring instead of ultrasound irradiation. As shown in Figure 5f, the products are mainly small particles along with some spherical congregations. The experiments proved that ultrasound irradiation was favorable for the formation of Znq_2 nanorods with uniform shape.

On the basis of the experimental results, a possible formation mechanism is proposed in Figure 6. The formation of rod-like Znq_2 in the W/O microemulsion may undergo various processes including small particle growth, fusion, and aggregation. The aqueous droplets containing the initial Znq_2 nuclei in the microemulsion underwent a collision and fusion process induced by the ultrasonic irradiation. With the reaction proceeding, the fused particles would be enlarged and further grow in the microemulsion. After collision and fusion of W/O microemulsion droplets covered with surfactant layers, The Znq_2 nanorods can be obtained.

Protein Sensing. The excitation and emission spectra for the Znq_2 nanorods are shown in Figure 7a. Maximal excitation and emission wavelength occurred at 338 and 487 nm, respectively. The as-prepared Znq_2 nanorods have a large Stokes shift as compared with conventional dye probes, such as fluorescein, rhodamine B, and acridine orange (most with a Stokes shift

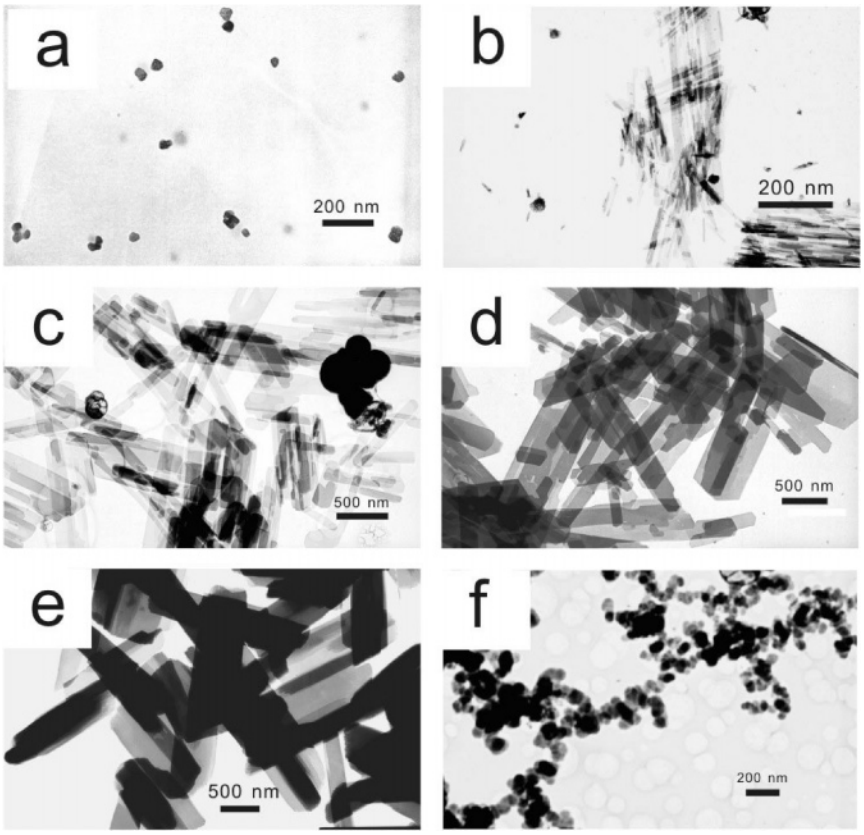

Figure 5. TEM images of the products obtained at different reaction conditions: after ultrasound treatment for (a) 1, (b) 3, (c) 6, (d) 12, and (e) 40 min; under electromagnetic stirring instead of ultrasound treatment for (f) 45 min.

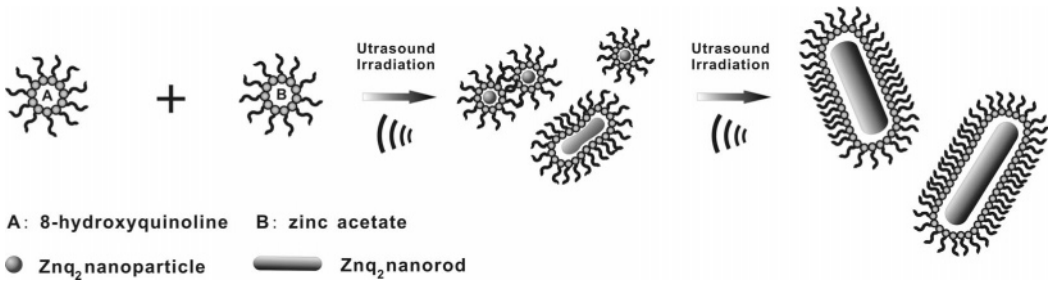

Figure 6. Schematic illustration of the formation mechanism of the Znq_2 nanorods.

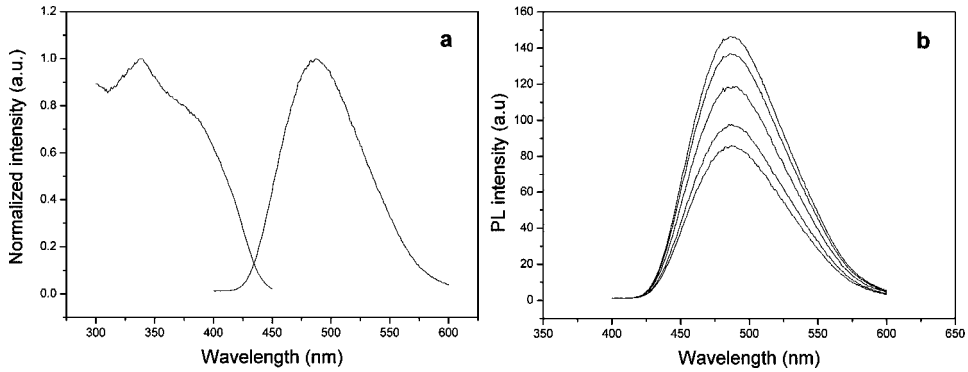

Figure 7. (a) The excitation and emission spectra of the Znq_2 nanorods in a NaAc−HAc buffer solution (20 mM, pH 4.2). (b) The PL spectra of the Znq_2 nanorods in a NaAc−HAc buffer solution (20 mM, pH 4.2) and upon addition of an increasing amount of HSA (0, 8, 20, 40, and 80 ng mL^{-1}).

less than 50 nm). Therefore Znq_2 nanorods could serve as an ideal candidate for applications in protein sensing. The photoluminescence intensity of Znq_2 nanorods increases considerably in a 20 mM NaAc−HAc buffer solution containing protein (e.g., HSA, BSA, Hb, or EA) at pH 4.2. Figure 7b shows that the PL intensity of Znq_2 nanorods increases by about 170% in a solution containing 80 ng mL^{-1} of HSA, as compared to the emission of these Znq_2 nanorods in a HSA-free solution. Figure 8a describes the HSA concentration dependence of the PL intensity of Znq_2 nanorods. It can be observed that the PL intensity of Znq_2 nanorods increases sharply in response to HSA. The detection limit is ~4 ng mL^{-1}, and the dynamic range is up to

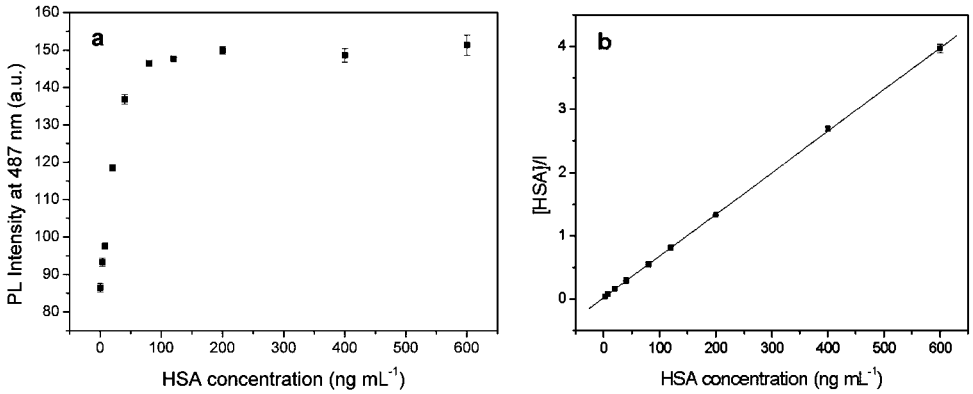

Figure 8. (a) The PL intensity ($\lambda_{ex} = 338$ nm, $\lambda_{em} = 487$ nm) vs equivalents of added HSA for the Znq_2 nanorods in a NaAc−HAc buffer solution (20 mM, pH 4.2). (b) Langmuir binding isotherm description of the data showing a linear fit throughout the HSA concentration range, with a binding constant of 0.25 and a correlation coefficient $r^2 = 0.9992$.

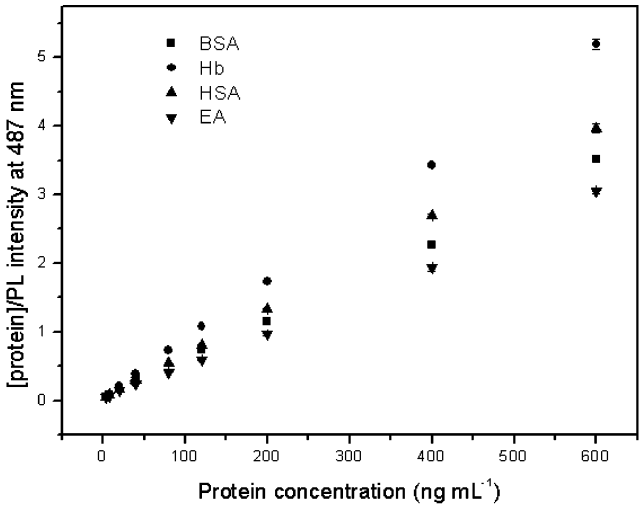

Figure 9. The ratio of the protein to the PL intensity at 487 nm vs the proteins.

40 ng mL^{-1}. In previous studies, Rosenzweig and Chen reported that the binding of zinc ions to the surface of the CdS quantum dots results in the emission enhancement of the quantum dots.[33] They described the zinc ion concentration dependence of the luminescence intensity using a Langmuir-type binding model. In this study, we found that the PL intensity of Znq_2 nanorods enhances as the protein concentration increases. Interestingly, the protein-concentration dependence of the PL intensity can be effectively described by a Langmuir-type binding isotherm, closely resembling the emission enhancement behavior of zinc ions on the quantum dots. The protein-enhanced PL intensity of the Znq_2 nanorods could be attributed to activation of surface states of Znq_2 nanorods by protein binding. Figure 8a shows that the PL intensity sharply increases as the HSA concentration increases to 120 ng mL^{-1} and then levels off at a HSA concentration of more than 200 ng mL^{-1}, due to the decreasing availability of binding sites on the surface of Znq_2 nanorods. According to the literature,[33] the surface of the Znq_2 nanorods affords a finite number of binding sites. Each of the binding sites could absorb one HSA molecule from the solution. The fraction of occupied sites is defined as Θ. The rate of binding of HSA to the surface is proportional to the HSA concentration C in the solution and to the fraction of available binding sites $1 - \Theta$. The rate of binding, R_b, of HSA to the surface is expressed as

$$R_b = K_b C(1 - \Theta) \tag{1}$$

where K_b is binding rate constant for HSA. The rate of desorption of bound HSA from the surface is independent of HSA concentration and depends only on the fraction of occupied binding sites. When the rate of binding is equal to the rate of desorption at equilibrium, the Langmuir isotherm can be written as:

$$K_d\Theta = K_b C(1 - \Theta) \tag{2}$$

The equation can be solved for Θ as a function of the ratio $B = K_b/K_d$.

$$\Theta = \frac{BC}{1 + BC} \tag{3}$$

The fraction of occupied binding sites, Θ, is related to the ratio between the signal obtained at a given protein concentration I and the maximum intensity I_{max}.

$$\Theta = I/I_{max} \tag{4}$$

From eqs 3 and 4, the following equation can be obtained:

$$\frac{I}{I_{max}} = \frac{BC}{1 + BC} \tag{5}$$

This equation could be linearized to take the form

$$\frac{C}{I} = \frac{1}{BI_{max}} + \frac{1}{I_{max}}C \tag{6}$$

Accordingly, if the Langmuir description of the binding of HSA on the surface of the Znq_2 nanorods is correct, the dependence of C/I on the value of C should be linear, where C is the HSA concentration and I is the PL intensity of the Znq_2 nanorods at given HSA concentrations. As shown in Figure 8b, a very high linearity of the plot of C/I against C is observed throughout the entire range of HSA concentration. The binding constant B is found to be 0.25, and the correlation coefficient (r) of the linear fit is higher than 0.999. The PL enhancement behavior of BSA, Hb, and EA on the Znq_2 nanorods resembled that of HSA. As shown in Figure 9, the protein-concentration dependence of the PL intensity can be effectively described by the Langmuir binding isotherm.

In addition to enhanced PL emission, an increase in the RLS intensity of Znq_2 nanorods was also observed in the presence of HSA, BSA, Hb, or EA. Figure 10 shows the RLS spectra of the Znq_2 nanorods and upon addition of an increasing amount of HSA. The inset in Figure 9a depicts the HSA concentration

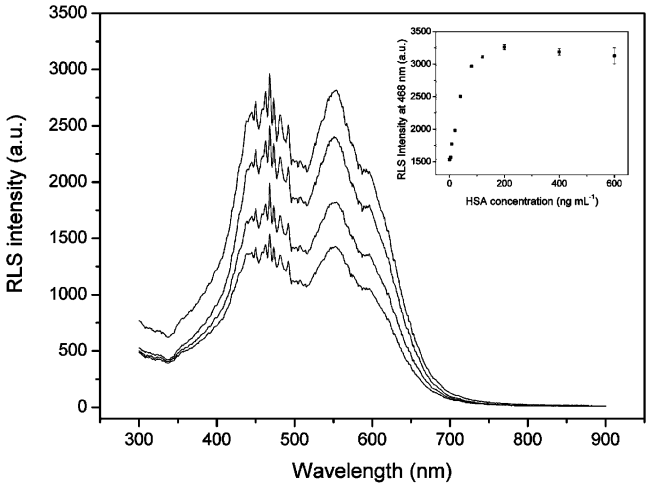

Figure 10. The RLS spectra of the Znq_2 nanorods in a NaAc−HAc buffer solution (20 mM, pH 4.2) and upon addition of an increasing amount of HSA (0, 8, 20, 40, and 80 ng mL^{-1}). Inset: The RLS intensity at 468 nm vs equivalents of added HSA for the Znq_2 nanorods in a NaAc−HAc buffer solution (20 mM, pH 4.2).

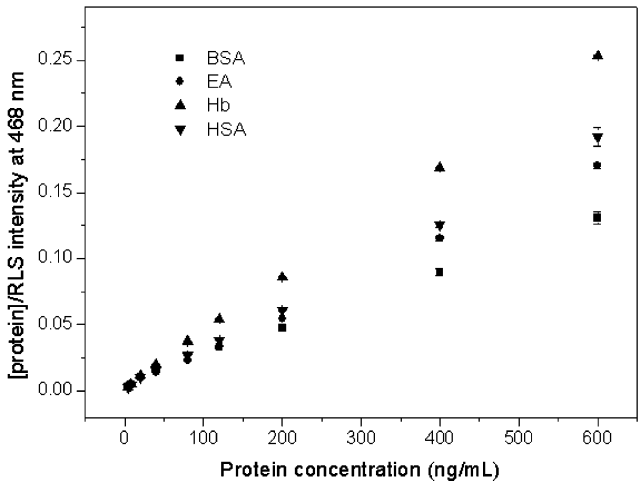

Figure 11. The ratio of the protein to the RLS intensity at 487 nm vs the proteins.

dependence of the RLS intensity at 468 nm for the Znq_2 nanorods. The HSA concentration dependence of the RLS intensity could be described by using a Langmuir-type binding model. According to eq 6, the dependence of C/I as function of C, where C is the concentration of HSA, BSA, Hb, and EA, and I is the RLS intensity of the Znq_2 nanorods at given protein concentrations, is shown in Figure 11.

Conclusions

In summary, a rapid sonochemical route combined with a microemulsion technique has been developed to synthesize luminescent Znq_2 nanorods. As we have demonstrated, the effect of ultrasound on the microemulsion directs the collision and fusion of the droplets, and the growth of Znq_2 in the droplets leads to the formation of the final rod-like morphology. These luminescent nanorods have a large Stokes shift (about 150 nm) and therefore could be used as an attractive alternative for protein sensing and other biological assays. We investigated the enhanced effect of four types of proteins (HSA, BSA, Hb, and EA) on the PL and the RLS intensity. The protein-concentration dependence of both the PL and the RLS intensities can be effectively described as a Langmuir-type binding isotherm. These Znq_2 nanorods exhibited highly sensitive signals involving PL and RLS for protein, allowing one to detect HSA at the nanogram per milliliter level. It is expected that these Znq_2 complex nanorods may open a new route for design of optical biosensors. Current efforts are directed toward elucidating the surface effect of the Znq_2 nanorods on the optical performance in detail and to designing optical sensors for immunoassays.

Acknowledgment. We greatly appreciate the support of the National Natural Science Foundation of China (Nos. 20325516, 20635020, 90606016, 90206037). This work is also supported by the NSFC for Creative Research Group (20521503).

References and Notes

(1) Bruchez, M., Jr.; Moronne, M.; Gin, P.; Weiss, S.; Alivisatos, A. P. *Science* **1998**, *281*, 2013.
(2) Chan, W. C. W.; Nie, S. *Science* **1998**, *281*, 2016.
(3) Wuister, S. F.; Swart, I.; van Driel, F.; Hickey, S. G.; de Mello Donega, C. *Nano Lett.* **2003**, *3*, 503.
(4) Han, W. S.; Kang, Y.; Lee, S. J.; Lee, H.; Do, Y.; Lee, Y.-A.; Jung, J. H. *J. Phys. Chem. B* **2005**, *109*, 20661.
(5) Harma, H.; Soukka, T.; Lovgren, T. *Clin. Chem.* **2001**, *47*, 561.
(6) Wang, L. Y.; Li, Y. D. *Chem. Commun.* **2006**, 2557.
(7) Wang, L. Y.; Yan, R. X.; Hao, Z. Y.; Wang, L.; Zeng, J. H.; Bao, H.; Wang, X.; Peng, Q.; Li, Y. D. *Angew. Chem., Int. Ed.* **2005**, *44*, 6054.
(8) Zeng, J. H.; Su, J.; Li, Z. H.; Yan, R. X.; Li, Y. D. *Adv. Mater.* **2005**, *17*, 2119.
(9) Berenguer, J. R.; Forniés, J.; Gil, B.; Lalinde, E. *Chem. Eur. J.* **2006**, *12*, 785.
(10) Lo, K. K-W.; Chung, C.-K.; Zhu, N. *Chem. Eur. J.* **2006**, *12*, 1500.
(11) Farruggia, G.; Iotti, S.; Prodi, L.; Montalti, M.; Zaccheroni, N.; Savage, P. B.; Trapani, V.; Sale, P.; Wolf, F. I. *J. Am. Chem. Soc.* **2006**, *128*, 344.
(12) Song, J.-L.; Mao, J.-G. *Chem. Eur. J.* **2005**, *11*, 1417.
(13) Tsolakis, P. K.; Kallitsis, J. K. *Chem. Eur. J.* **2003**, *9*, 936.
(14) Wong, K-H.; Chan, M. C.-W.; Che, C.-M. *Chem. Eur. J.* **1999**, *5*, 2845.
(15) Sapochak, L. S.; Benincasa, F. E.; Schofield, R. S.; Baker, J. L.; Riccio, K. K. C.; Fogarty, D.; Kohlmann, H.; Ferris, K. F.; Burrows, P. E. *J. Am. Chem. Soc.* **2002**, *124*, 6119.
(16) Sapochak, L. S.; Falkowitz, A.; Ferris, K. F.; Steinberg, S.; Burrows, P. E. *J. Phys. Chem. B* **2004**, *108*, 8558.
(17) Jonda, C.; Mayer, A. B.; Stolz, U. *J. Mater. Sci.* **2000**, *35*, 5645.
(18) Yu, G.; Yin, S.; Liu, Y. Q.; Chen, J.; Xu, X.; Sun, X.; Ma, D.; Zhan, X.; Peng, Q.; Shuai, Z. G.; Tang, B. Z.; Zhu, D. B.; Fang, W.; Luo, Y. *J. Am. Chem. Soc.* **2005**, *127*, 6335.
(19) Yu, G.; Liu, Y.; Zhou, S.; Bai, F.; Zeng, P.; Zheng, M.; Wu, X.; Zhu, D. *Phys. Rev. B* **2002**, *65*, 115211.
(20) Mandoc, M. M.; de Boer, B.; Blom, P. W. M. *Phys. Rev. B* **2006**, *73*, 155205.
(21) Qiu, X.; Burda, C.; Fu, R.; Pu, L.; Chen, H.; Zhu, J. *J. Am. Chem. Soc.* **2004**, *126*, 16276.
(22) Zhu, J.-J.; Xu, S.; Wang, H.; Chen, H.-Y. *Adv. Mater.* **2003**, *15*, 156.
(23) Geng, J.; Hou, W.-H.; Lv, Y.-N.; Zhu, J.-J.; Chen, H.-Y. *Inorg. Chem.* **2005**, *44*, 8503.
(24) Geng, J.; Zhu, J.-J.; Chen, H.-Y. *Cryst. Growth Des.* **2006**, *6*, 321.
(25) Wang, H.; Zhu, J.-J.; Zhu, J.-M.; Chen, H.-Y. *J. Phys. Chem. B* **2002**, *106*, 3848.
(26) Jiang, L.-P.; Xu, S.; Zhu, J.-M.; Zhang, J.-R.; Zhu, J.-J.; Chen, H.-Y. *Inorg. Chem.* **2004**, *43*, 5877.
(27) Miao, J.-J.; Fu, R.-L.; Zhu, J.-M.; Xu, K.; Zhu, J.-J.; Chen, H.-Y. *Chem. Commun.* **2006**, 3013.
(28) Mao, C.-J.; Pan, H.-C.; Wu, X.-C.; Zhu, J.-J.; Chen, H.-Y. *J. Phys. Chem. B* **2006**, *110*, 14709.
(29) Phillips, J. P.; Deye, J. F. *Anal. Chim. Acta* **1957**, *17*, 231.
(30) Gavrilko, T.; Fedorovich, R.; Dovbeshko, G.; Marchenko, A.; Naumovets, A.; Nechytaylo, V.; Puchkovska, G.; Viduta, L.; Baran, J.; Ratajczak, H. *J. Mol. Struct.* **2004**, *704*, 163.
(31) Tackett, J. E.; Sawyer, D. T. *Inorg. Chem.* **1964**, *3*, 692.
(32) Engelter, C.; Jackson, G. E.; Knight, C. L.; Thornton, D. A. *J. Mol. Struct.* **1983**, *213*, 133.
(33) Chen, Y.; Rosenzweig, Z. *Anal. Chem.* **2002**, *74*, 5132.